Commun. Comput. Phys.
doi: 10.4208/cicp.160811.270212a

Vol. **13**, No. 2, pp. 479-501
February 2013

Conservative Residual Distribution Method for Viscous Double Cone Flows in Thermochemical Nonequilibrium

Andrea Lani[1,*], Marco Panesi[2] and Herman Deconinck[1]

[1] *Von Karman Institute for Fluid Dynamics, Waterloosesteenweg 72, 1640, Sint Genesius Rode, Belgium.*
[2] *Institute for Computational Engineering and Sciences, University of Texas, Austin, Texas 78712, USA.*

Received 16 August 2011; Accepted (in revised version) 27 February 2012

Available online 28 June 2012

Abstract. A multi-dimensionally upwind conservative Residual Distribution algorithm for simulating viscous axisymmetric hypersonic flows in thermo-chemical nonequilibrium on unstructured grids is presented and validated in the case of the complex flowfield over a double cone configuration. The resulting numerical discretization combines a state-of-the-art nonlinear quasi-monotone second order blended scheme for distributing the convective residual and a standard Galerkin formulation for the diffusive residual. The physical source terms are upwinded together with the convective fluxes. Numerical results show an excellent agreement with experimental measurements and available literature.

PACS: 47.40.Ki, 47.70.Nd, 47.11.-j, 47.11.Fg

Key words: Unstructured mesh, hypersonic flows, thermo-chemical nonequilibrium, residual distribution schemes, double cone.

1 Introduction

During the last three decades, remarkable progress has been made in the development of algorithms for the numerical simulation of complex fluid dynamic phenomena, while the concurrent growth of resources for parallel and distributed computing have pushed researchers to devote their efforts towards more challenging applications. The accurate simulation of high-enthalpy hypersonic flows in thermal and chemical nonequilibrium,

*Corresponding author. *Email addresses:* lani@vki.ac.be (A. Lani), mpanesi@ices.utexas.edu (M. Panesi), deco@vki.ac.be (H. Deconinck)

however, still remains extremely challenging from a computational point of view, particularly on unstructured grids. For this kind of application, the Finite Volume (FV) method [3, 11, 25, 31] has consolidated itself as the *de facto* standard technique and a reliable alternative to it has yet to be found.

Over the past decade, however, multi-dimensional upwind Residual Distribution (RD) schemes have proved to be an attractive alternative to the classical FV upwind approach based on one-dimensional Riemann solvers for the simulation of compressible flows [4,7,9,14,32]. The main advantages of RD schemes include (1) an outstanding shock capturing (due to the lower cross diffusion associated to a truly multi-dimensional upwinding and to the positivity property) and (2) a compact stencil for ensuring a linearity preserving resolution. The latter does not require expensive polynomial reconstructions based on enlarged stencils in order to guarantee second order accuracy and supports an easy and efficient parallelization [6, 36, 37].

Following a previous unique attempt to apply RD schemes to 2D inviscid chemical nonequilibrium high-speed flows [8], in this paper, the RD method is extended and adapted for simulating viscous flows in thermal and chemical nonequilibrium in complex 2D axisymmetric cases with a two-temperature model.

Unlike in [8], the convective terms of the equations are discretized by means of a strictly conservative formulation of the standard RD method, denominated Contour Residual Distribution (CRD) [5, 32], which is based on a redefinition of the positive system N scheme, the so-called Nc scheme. The latter conveniently does not require a specific set of variables (e.g. Roe parameter vector in [8]) for the linearization of the flux jacobian, at the price of an additional contour integration of the convective flux in each computational cell. Second order accuracy is obtained by means of a blended Nc/LDAc (Bxc) scheme [9,10], where the blending coefficient depends on a shock capturing sensor based on a user-defined flow variable. This second order scheme, which is presented to the reader in Section 3, is as compact as the first order one, which make it really suitable for a parallel solver. Since only the closest cell neighbors are needed, parallelization only requires one single layer of cells in the overlap region between contiguous processors. The diffusive fluxes are discretized with a standard Galerkin approach [6], while the source terms are upwinded together with the convective fluxes.

The resulting system of discrete equations is driven to steady state convergence by means of a fully implicit first-order accurate in time backward Euler scheme, which employs a preconditioned Generalized Minimum Residual (GMRES) algorithm [30] to solve linear systems arising from the corresponding Newton linearization. The parallel implicit numerical solver has been implemented within COOLFluiD[†], a collaborative multi-physics platform [16, 17] developed at the Von Karman Institute for Fluid Dynamics during the last ten years.

The article will be organized as follows: first, the multi-temperature thermo-chemical nonequilibrium model is reviewed; second, the residual distribution method is described

[†]Computational Object Oriented Libraries for Fluid Dynamics

in details; third, some numerical results of the RD method on a challenging double cone configuration are discussed and validated against experimental data. A comparison against a reference numerical solution available in literature, corresponding to a state-of-the-art cell-centered FV code [26], is also addressed.

2 Thermo-chemical nonequilibrium model

The system of governing equations for a gas mixture in thermal and chemical nonequilibrium in an axisymmetric case can be expressed as follows:

$$\frac{\partial \mathbf{U}}{\partial \mathbf{P}}\frac{\partial \mathbf{P}}{\partial t}+\frac{\partial \mathbf{F^c}}{\partial x}+\frac{\partial \mathbf{G^c}}{\partial r}=\frac{\partial \mathbf{F^d}}{\partial x}+\frac{\partial \mathbf{G^d}}{\partial r}+\mathbf{S}, \tag{2.1}$$

with the following definitions for the conservative $\mathbf{U}$ and the natural $\mathbf{P}$ variables:

$$\mathbf{U}=[\rho_s\ \rho u\ \rho v\ \rho E\ \rho e_v]^T, \qquad \mathbf{P}=[\rho_s\ u\ v\ T\ T_v]^T, \tag{2.2}$$

where ρ_s are the partial densities, ρ is the mixture density, u and v are the longitudinal and radial velocity components, E the total energy per unit mass, e_v the vibrational energy per unit mass, T and T_v the roto-translational and vibrational temperatures respectively. The convective fluxes $\mathbf{F^c}$ and $\mathbf{G^c}$ are given by

$$\mathbf{F^c}=\begin{pmatrix}\rho_s u\\ \rho u u+p\\ \rho u v\\ \rho u H\\ \rho u e_v\end{pmatrix}, \qquad \mathbf{G^c}=\begin{pmatrix}\rho_s v\\ \rho u v\\ \rho v v+p\\ \rho v H\\ \rho v e_v\end{pmatrix}, \tag{2.3}$$

where $H=E+p/\rho$ is the total enthalpy per unit mass and p is the mixture pressure which is given by Dalton's law, assuming that each species behaves as a perfect gas:

$$p=\sum_s p_s=R\ T\sum_s \frac{\rho_s}{M_s}, \tag{2.4}$$

with R being the universal gas constant and M_s the species molar masses.

The diffusive fluxes $\mathbf{F^d}$ and $\mathbf{G^d}$ read

$$\mathbf{F^d}=\begin{pmatrix}-\rho_s u_s\\ \tau_{xx}\\ \tau_{xr}\\ \tau_{xx}u+\tau_{xr}v-(q_x+q_x^v)-\sum_s \rho_s u_s h_s\\ -q_x^v-\sum_s \rho_s u_s h_s^v\end{pmatrix}, \tag{2.5}$$

$$\mathbf{G^d}=\begin{pmatrix}-\rho_s v_s\\ \tau_{xr}\\ \tau_{rr}\\ \tau_{xr}u+\tau_{rr}v-(q_r+q_r^v)-\sum_s \rho_s v_s h_s\\ -q_r^v-\sum_s \rho_s v_s h_s^v\end{pmatrix}, \tag{2.6}$$

where r is the radius, which in the present case coincides with the y distance from the symmetry axis. Finally, the source term $\mathbf{S}$ is defined as

$$\mathbf{S}=-\frac{1}{r}\begin{pmatrix}\rho_s v\\ \rho uv\\ \rho v^2\\ \rho vH\\ \rho v e_v\end{pmatrix}+\frac{1}{r}\begin{pmatrix}\rho_s v_s\\ \tau_{rx}\\ \tau_{rr}-\tau_{\theta\theta}\\ \tau_{rx}\,u+\tau_{rr}\,v-(q_r+q_r^v)-\sum_s\rho_s v_s h_s\\ -q_r^v-\sum_s\rho_s v_s h_s^v\end{pmatrix}+\begin{pmatrix}\dot{\omega}_s\\ 0\\ 0\\ 0\\ \dot{\omega}_v\end{pmatrix}. \tag{2.7}$$

Under Stokes' hypothesis of negligible bulk viscosity effects, the viscous stresses can be expressed as follows:

$$\tau_{ij}=\mu\left(\frac{\partial u_j}{\partial x_i}+\frac{\partial u_i}{\partial x_j}\right), \tag{2.8}$$

$$\tau_{ii}=2\mu\frac{\partial u_i}{\partial x_i}-\frac{2}{3}\mu\left(\frac{\partial u}{\partial x}+\frac{\partial v}{\partial r}+\frac{v}{r}\right), \tag{2.9}$$

$$\tau_{\theta\theta}=-\frac{2}{3}\mu\left(\frac{\partial u}{\partial x}+\frac{\partial v}{\partial r}-2\frac{v}{r}\right), \tag{2.10}$$

where $\tau_{\theta\theta}$ are the viscous stress components in the circumferential direction θ. The heat fluxes appearing in (2.5)-(2.7) are defined as

$$q_j=-(\lambda_t+\lambda_r)\frac{\partial T}{\partial x_j},\qquad q_j^v=-\lambda_v\frac{\partial T_v}{\partial x_j}. \tag{2.11}$$

The modified Chapman-Enskog pertubative analysis for partially ionized plasmas presented in [20] is the basis for the computation of transport coefficients and fluxes. Efficient iterative algorithms presented in [19] are used to solve the linear systems for the shear-viscosity μ and the translational thermal conductivity λ_t. This is not only more accurate but also computationally cheaper than using mixture rules such as Yos' [38] as is the case in many high Mach number high-enthalpy solvers. The rotational λ_r and vibrational λ_v thermal conductivities are modelled by means of the Eucken approximation [13]. Mass diffusion fluxes $\rho_s\mathbf{u}_s$ are computed by solving the Stefan-Maxwell equations as in [1].

The mass production/destruction term for chemical species $\dot{\omega}_s$ which appears in (2.1) is formulated as follows:

$$\dot{\omega}_s=M_s\sum_{r=1}^{Nr}\left(\nu_{sr}^{''}-\nu_{sr}^{'}\right)\left\{k_{fr}\prod_{j=1}^{Ns}\left(\frac{\rho_j}{M_j}\right)^{\nu_{jr}^{'}}-k_{br}\prod_{j=1}^{Ns}\left(\frac{\rho_j}{M_j}\right)^{\nu_{jr}^{''}}\right\}, \tag{2.12}$$

where ν are stoichiometric coefficients and the forward reaction rates coefficients

$$k_{fr}=A_{f,r}T_1^{n_{f,r}}exp(-E_{f,r}/k\,T_1), \tag{2.13}$$

are expressed by means of Arrhenius' law. In the latter, the constants $A_{f,r}$, $n_{f,r}$ and $E_{f,r}$ are provided by chemical kinetic models such as [12, 28] in the case of air mixtures and

T_1 is the rate controlling temperature which is empirically defined as $T_1=\sqrt{TTv}$ in [28]. The backward reactions rates are computes as

$$k_{b,r}=k_{f,r}/K_{c,r}^{eq}, \tag{2.14}$$

where $K_{c,r}^{eq}$ is the equilibrium reaction rate constant.

As far as energy transfer is concerned, in the two-temperature model for neutral mixtures used in this work, $\dot{\omega}_v$ reads

$$\dot{\omega}_v=\sum_s \rho_s \frac{(e_{v,s}^*-e_{v,s})}{\tau_s}+\sum_s \tilde{D}_s\dot{\omega}_s. \tag{2.15}$$

This includes two contributions: (1) the energy exchange between vibrational and translational modes according to Landau Teller formulation and (2) the vibrational energy lost or gained due to molecular depletion (dissociation) or production (recombination). In (1), $e_{v,s}^*$ is the equilibrium vibrational energy of the molecule evaluated at the roto-translational temperature and τ_s are the relaxation times given by Millikan and White [21] with Park's correction for high temperatures [29]:

$$\tau_s=\tau_s^{MW}(p,T)+\overbrace{(\sigma_s c_s n_s)^{-1}}^{\tau_{Park}}, \tag{2.16}$$

where σ_s is the effective cross section for vibrational relaxation processes, c_s is the average molecular velocity of molecule s and n_s is the number density.

The quantity $\tilde{D}_s$ in (2) is imposed equal to the vibrational energy of the molecule, namely

$$\tilde{D}_s=e_{v,s}. \tag{2.17}$$

For a broader introduction to the thermodynamic and transport properties modeling employed in this work, the reader may refer to [1,2,11,19,20,31,35].

3 Residual distribution method

3.1 General concepts

Let the computational domain be subdivided into linear triangles with unknowns defined at the vertexes. Assuming a Finite Element (FE) framework, the solution inside a triangle can be represented as

$$\mathbf{P}^h(\mathbf{x},t)=\sum_{j=1}^{3}\mathbf{P}_j(t)N_j(\mathbf{x}), \qquad N_j(\mathbf{x}_k)=\delta_{jk}, \tag{3.1}$$

where an example of linear shape functions $N_j(\mathbf{x})$ is depicted in Fig. 1 (left).

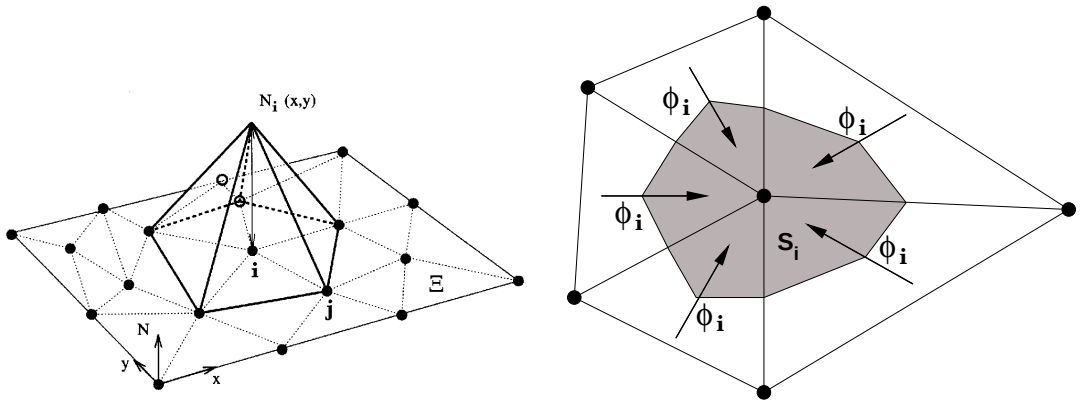

Figure 1: Linear shape function associated to a triangle (left) and median dual cell surrounding a node (right) in a vertex centered discretization.

The basic idea of the RD algorithm consists in distributing fractions of the residual, defined by integrating the spatial part of (2.1) over a given cell (or element), to the nodes of the same cell, taking into account the directions of propagation of the physical signals, according to an upwind philosophy. The semi-discretized form of (2.1) for a vertex l, assuming a lumped mass matrix [37], becomes:

$$\frac{\partial \mathbf{U}}{\partial \mathbf{P}}(\mathbf{P}_l)\frac{d\mathbf{P}_l}{dt}\Omega_l + \mathbf{\Phi}_l^c = \mathbf{\Phi}_l^d + \mathbf{\Phi}_l^S, \tag{3.2}$$

where $\mathbf{\Phi}_l^c$, $\mathbf{\Phi}_l^d$ and $\mathbf{\Phi}_l^S$ are the three different nodal residuals corresponding respectively to convective, diffusive and source terms. Ω_l is the area of the median dual cell, as shown in Fig. 1 (right) for a mesh composed of triangles. Due to the lumping of the mass matrix, accuracy in time is reduced to first order in (3.2). Each of the three residuals in (3.2) are now analyzed in more detail.

3.2 Convective term discretization

Consider the system of PDE's in (2.1) and rewrite the convective term in quasi-linear form:

$$\frac{\partial \mathbf{F}_i^c}{\partial x_i} = \mathbf{A}_i \frac{\partial \mathbf{U}}{\partial x_i}, \tag{3.3}$$

where $\mathbf{A}_i$ are non-commuting $N \times N$ jacobian matrices, if N is the size of the state vector $\mathbf{U}$. For a given node in a triangle, the generalized upwind parameters $\mathbf{K}_l$ can be expressed as follows [37]:

$$\mathbf{K}_l = \frac{1}{2}\bar{\mathbf{A}}_i n_{l_i} = \frac{1}{2}\mathbf{R}_l \mathbf{\Lambda}_l \mathbf{L}_l, \tag{3.4}$$

where $\bar{\mathbf{A}}_i n_{l_i}$ are the projected Jacobians evaluated in a conservative linearized state and n_{l_i} is the i component of the inward normal scaled with the area of the face opposite

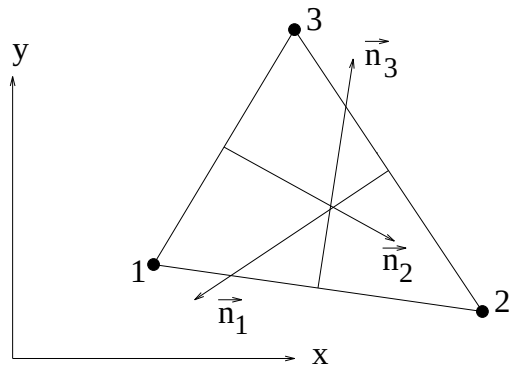

Figure 2: Inward scaled normals in a triangle.

to node l. In the case of a triangle with counter clockwise node numbering, the three normals are shown in Fig. 2 and are defined by:

$$\mathbf{n}_1 = (y_2 - y_3)\vec{1}_x + (x_3 - x_2)\vec{1}_y, \tag{3.5}$$

$$\mathbf{n}_2 = (y_3 - y_1)\vec{1}_x + (x_1 - x_3)\vec{1}_y, \tag{3.6}$$

$$\mathbf{n}_3 = (y_1 - y_2)\vec{1}_x + (x_2 - x_1)\vec{1}_y. \tag{3.7}$$

Since the system is hyperbolic in time, the so-called upwind matrix $\mathbf{K}_l$ has a complete set of real eigenvalues and eigenvectors. The columns of $\mathbf{R}_l$ contain the right eigenvectors, $\mathbf{\Lambda}_l$ is a diagonal matrix of the eigenvalues and $\mathbf{L}_l = \mathbf{R}_l^{-1}$. The analytical expressions for $\mathbf{R}_l$, $\mathbf{L}_l$, $\mathbf{\Lambda}_l$ in the specific case of a mixture of perfect gases in thermal and chemical nonequilibrium can be found in [11,31]. The split matrices $\mathbf{K}_l^+$ and $\mathbf{K}_l^-$ are defined as:

$$\mathbf{K}_l^+ = \frac{1}{2}\mathbf{R}_l\mathbf{\Lambda}_l^+\mathbf{L}_l, \qquad \mathbf{K}_l^- = \frac{1}{2}\mathbf{R}_l\mathbf{\Lambda}_l^-\mathbf{L}_l, \tag{3.8}$$

with $\mathbf{\Lambda}_l^+$ and $\mathbf{\Lambda}_l^-$ containing the positive and negative eigenvalues.

The nodal residual is computed by gathering the contributions of all neighbor cell residuals:

$$\mathbf{\Phi}_l^c = \sum_{\Omega \in \Xi_l} \mathbf{B}_l^\Omega \mathbf{\Phi}^{c,\Omega}, \tag{3.9}$$

where Ξ_l is the set of neighboring cells sharing node l and $\mathbf{B}_l^\Omega$ are the so-called *distribution matrices*, which define the fraction of residual $\mathbf{\Phi}^{c,\Omega}$ sent to node l inside each element with area Ω, i.e. $\sum_{l\in\Omega}\mathbf{B}_l^\Omega = \mathbf{I}$. The actual expression for $\mathbf{B}$ depends on the split upwind matrices defined in (3.8) and varies from one to another distributive scheme. Herein, the convective cell residual $\mathbf{\Phi}^{c,\Omega}$ in (3.9) is given by

$$\mathbf{\Phi}^{c,\Omega} = \int_\Omega \mathbf{A}_i \frac{\partial \mathbf{U}}{\partial x_i} d\Omega = \oint_{\partial\Omega} \mathbf{A}_i n_i^{\text{ext}} \mathbf{U} d\partial\Omega. \tag{3.10}$$

The original RD formulation [6,7,36], a.k.a. Linear Residual Distribution (LRD), assumes $\mathbf{A}_i$ is constant per cell and a linear variation of U on each element, which leads to the following simplified expression for the convective cell residual:

$$\mathbf{\Phi}^{c,\Omega} = \sum_{j=1}^{3} \mathbf{K}_j \mathbf{U}_j = \tilde{\mathbf{\Phi}}^{c,\Omega}. \tag{3.11}$$

3.2.1 Conservative residual distribution

LRD can be employed only if a conservative linearization based on a Roe-like average state vector is available for the Jacobians of the convective fluxes, but unfortunately this is not applicable to our case. However, it has been demonstrated [5, 32] that the RD schemes can be reformulated so that conservation is retained independently from the variables chosen to linearize the cell Jacobians. The novel formulation, denominated *CRD* (Contour Residual Distribution), requires an additional contour integration of the fluxes in the element, i.e. the calculation of the residual by means of an appropriate quadrature rule:

$$\Phi^{c,\Omega} = \oint_{\partial\Omega} \vec{\mathbf{F}}^c \cdot \vec{n} \, d\partial\Omega. \tag{3.12}$$

As demonstrated in [4], the CRD version of the first order positive system N scheme can be expressed as the LRD counterpart with a generally *non* conservative linearization plus a conservation correction, defined in terms of an upwinded quantity

$$\delta\mathbf{\Phi}^{c,\Omega} = \mathbf{\Phi}^{c,\Omega} - \tilde{\mathbf{\Phi}}^{c,\Omega} \neq 0, \tag{3.13}$$

expressing the difference between (3.11) and (3.12):

$$\Phi_l^{Nc} = \tilde{\Phi}_l^N - \tilde{\mathbf{B}}_l^{LDA}(\tilde{\Phi}^{c,\Omega} - \Phi^{c,\Omega}), \tag{3.14}$$

$$\tilde{\Phi}_l^N = \tilde{\mathbf{K}}_l^+ (\mathbf{U}_l^c - \mathbf{U}_{in}). \tag{3.15}$$

Since a distribution coefficient cannot be explicitly defined for the N scheme, the conservation error in Eq. (3.13) is distributed with the second order LDA scheme in Eq. (3.14), whose distribution coefficient is given by:

$$\tilde{\mathbf{B}}_l^{LDA} = \tilde{\mathbf{K}}_l^+ \left(\sum_{j=1}^{3} \tilde{\mathbf{K}}_j^+ \right)^{-1}. \tag{3.16}$$

$\mathbf{U}_l^c$, appearing in Eq. (3.15), indicates the consistent nodal values of the distribution variables $\mathbf{U}_l$ and can be expressed as:

$$\mathbf{U}_j^c = \frac{\partial \mathbf{U}}{\partial \mathbf{Z}}(\bar{\mathbf{Z}}) \, \mathbf{Z}_j, \tag{3.17}$$

where $\mathbf{Z}$ are the arbitrary variables chosen for the jacobian linearization. This definition, first introduced in [37], satisfies

$$\frac{\partial \mathbf{U}^c}{\partial x_i} = \frac{\partial \mathbf{U}}{\partial \mathbf{Z}}(\bar{\mathbf{Z}}) \frac{\partial \mathbf{Z}}{\partial x_i} \tag{3.18}$$

at the cell level. The inflow parameter vector $\mathbf{U}_{in}$ appearing in (3.15) is defined as

$$\mathbf{U}_{in} = \left(\sum_{j=1}^{3} \tilde{\mathbf{K}}_j^- \right)^{-1} \left(\sum_{j=1}^{3} \tilde{\mathbf{K}}_j^- \mathbf{U}_j^c \right). \tag{3.19}$$

All upwind matrices are evaluated in a linearized state, i.e. $\tilde{\mathbf{K}}_l^{\pm} = \mathbf{K}_l^{\pm}(\bar{\mathbf{Z}})$.

The resulting Nc scheme, blending together a strictly monotone scheme (the LRD version of the N scheme) applied to the residual and a non-monotone scheme (LDA) used for distributing the conservation error, is non-strictly positive (i.e., *quasi-posive*) but fully conservative. The use of the CRD method allows us not to resort to relatively complex linearization techniques like those presented in [8] or [31] (in a FV context) which extend the usage of the Roe parameter vector to the case of gas mixtures in nonequilibrium. As an effect of the conservative nature of the Nc scheme, at least in principle, one can choose either the natural, or the primitive or the conservative variables to perform the flux jacobian linearization and still maintain conservation. In our experience, however, the linearization in conservative variables has shown to be more robust.

In the present work, $\tilde{\mathbf{B}}_l^{LDA}$ is also employed for the distribution of the source term which is subtracted from $\Phi^{c,\Omega}$:

$$\Phi_l^{Nc} = \tilde{\Phi}_l^N - \tilde{\mathbf{B}}_l^{LDA} \left[\tilde{\Phi}^{c,\Omega} - \left(\Phi^{c,\Omega} - \Phi^{S,\Omega} \right) \right]. \tag{3.20}$$

3.2.2 Bxc scheme

By using a non-linear blending of the distribution coefficients of a linearity preserving linear scheme like LDAc (which is second-order but non-positive) with the Nc-scheme (linear and quasi-monotone, but only first-order) a linearity preserving and quasi-monotone scheme can be obtained. The fraction of the element residual distributed to node i is defined as:

$$\Phi_l^{Bxc} = (1-\Theta)\Phi_i^{LDAc} + \Theta \Phi_i^{Nc}, \tag{3.21}$$

where Θ is based on an element-wise shock capturing sensor sc as proposed in [9,10]:

$$\Theta = \min(1, sc^2 h), \tag{3.22}$$

$$sc = \left(\frac{\nabla w \cdot \mathbf{v}}{\delta_{wv}} \right)^+ \approx \left(\frac{\sum_j w_j (\mathbf{n}_j \cdot \mathbf{v})}{d\, \Omega\, \delta_{wv}} \right)^+, \tag{3.23}$$

where w is a flow variable but not necessarily the pressure as in [9,10] (e.g. density has been the preferred choice in the present work, since it can also detect contact discontinuities); the term $\delta_{wv} \approx (w_{\max} - w_{\min}) \mid \bar{V} \mid$ is a global variation scale for w multiplied by

the magnitude of the mean velocity in the whole domain; h is the diameter of the circle whose area equals the area Ω of the considered element.

Fig. 3 shows the isolines of the density-based shock-sensor for the Bxc scheme on the double cone configuration. In most of the flowfield the pure second-order LDAc scheme is active. With the settings used in the actual simulation ($\delta\rho=0.52$), density gradients detected by the sensor are only located on the starting portion of the strong oblique shock on the leading edge, on the bow shock and on the transmitted shock region. This sharp detection of discontinuities leads to an overall accurate solution, even though a few overshoots in nodal roto-translational temperature are present due to the non-strict positivity of the Nc scheme. If more conservative settings for the shock-sensor are chosen (e.g. with $\delta\rho=0.052$, right picture in Fig. 3), the full shock structure can be clearly identified but the solution tends to be more dissipative. The value of $\delta\rho$ is critical for robustness purposes: in the present numerical experiments, $\delta\rho=0.52$ was the maximum value that could prevent the oscillatory behaviour of LDAc to manifest itself and instabilize the code at the prescribed initial CFL number ($=1$).

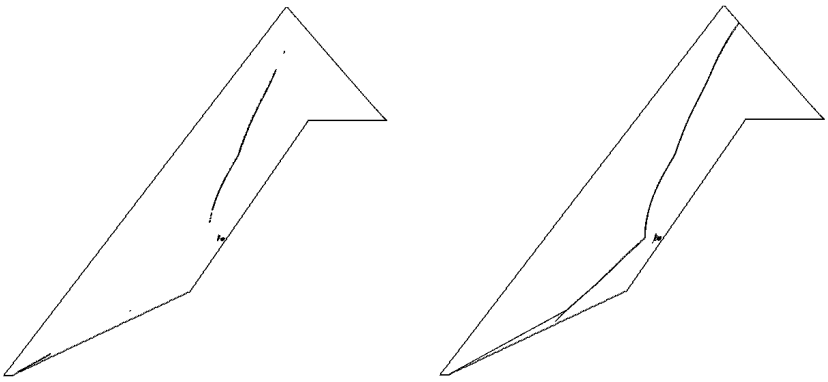

Figure 3: Density-based shock-sensor isolines with $\delta\rho=0.52$ (left) and with $\delta\rho=0.052$ (right).

The second order Bxc scheme uses only the nearest neighbor stencil and is therefore as compact as the first order Nc scheme, which makes it really suitable for parallel computing, since it only requires one single layer of shared cells in the overlap region between contiguous processors, i.e. one layer less than state-of-the-art second order Finite Volume algorithms.

3.3 Diffusive term discretization

As extensively explained in [6, 37], the whole residual distribution technique can be cast into a Petrov-Galerkin FE. In this section, starting from this analogy, the discretization of the diffusive terms is derived for the considered system of equations. The diffusive term in (2.1) is transformed into an equivalent variational formulation by multiplying it by the weight functions $\mathbf{w}_l(\mathbf{x})$ associated to an arbitrary node l and integrating the result

by parts over the whole domain Ξ:

$$\begin{aligned}\mathbf{\Phi}_l^d &= \int_\Xi \mathbf{w}_l \frac{\partial \mathbf{F}_i^d}{\partial x_i} d\Xi = \int_\Xi \frac{\partial}{\partial x_i}(\mathbf{w}_l \mathbf{F}_i^d)\, d\Xi - \int_\Xi \mathbf{F}_i^d \frac{\partial \mathbf{w}_l}{\partial x_i} d\Xi \\ &= \oint_{\partial\Xi} \mathbf{w}_l\, \mathbf{F}_i^d \cdot \mathbf{n}\, d\partial\Xi - \int_\Xi \mathbf{F}_i^d \frac{\partial \mathbf{w}_l}{\partial x_i} d\Xi, \end{aligned} \tag{3.24}$$

where $\mathbf{\Phi}_l^d$ is the fraction of diffusive flux which is distributed to node l. In particular, the last relation is due to the application of the Gauss theorem to the first volume integral, and the boundary integral vanishes for all interior nodes if homogeneous Dirichlet boundary conditions are assumed (as in our case). The remaining volume integral in (3.24) can be calculated as a summation over the individual elements in which the computational domain is subdivided, leading to the following definition for $\mathbf{\Phi}_l^d$ in (3.2):

$$\mathbf{\Phi}_l^d = -\sum_{\Omega\in\Xi_l} \int_\Omega \mathbf{F}_i^d \frac{\partial \mathbf{w}_l^\Omega}{\partial x_i} d\Omega. \tag{3.25}$$

If $\mathbf{w}_l$ are chosen to be Petrov-Galerkin weights, defined as

$$\mathbf{w}_l(\mathbf{x}) = \sum_{\Omega\in\Xi_l} \mathbf{w}_l^\Omega(\mathbf{x}) = N_l(\mathbf{x})\, \mathbf{I} + \sum_{\Omega\in\Xi_l} \left(\mathbf{B}_l^\Omega - \frac{1}{3}\mathbf{I}\right) \alpha^\Omega(\mathbf{x}), \tag{3.26}$$

where $N_l(\mathbf{x})$ is the nodal basis function in (3.1), $\mathbf{B}_l^\Omega$ are the distribution matrices and $\alpha^\Omega(\mathbf{x}) = 1$ inside element Ω and 0 outside, then $\frac{\partial \mathbf{w}_l}{\partial x_i} \equiv \frac{\partial N_l}{\partial x_i}\mathbf{I}$.

Here we assume a standard Galerkin method with $w_l(\mathbf{x}) = N_l(\mathbf{x})$. If the geometric relation $\frac{\partial N_l}{\partial x_i} = \frac{n_{li}}{2\Omega}$, which holds inside a linear simplex element, is taken into account, then (3.25) can be expressed as:

$$\mathbf{\Phi}_l^d = -\sum_{\Omega\in\Xi_l} \frac{1}{2\Omega} \int_\Omega \mathbf{F}^d \cdot \mathbf{n}_l\, d\Omega = -\sum_{\Omega\in\Xi_l} \frac{1}{2} (\mathbf{F}^d \cdot \mathbf{n}_l)(\bar{v}, \mathbf{n}_l, \bar{\mathbf{P}}, \nabla\tilde{\mathbf{P}}), \tag{3.27}$$

where $\bar{v}$ and $\bar{\mathbf{P}}$ represent respectively the array of transport properties and the update variables computed in the only quadrature point corresponding to a 1-point Gauss integration applied to the element. In this case, such a state also corresponds to the cell-averaged state which is used for the linearization of the jacobian matrices [27]. Moreover, $\mathbf{n}_l$ is the inward nodal normal and $\nabla\tilde{\mathbf{P}}$ are the gradients of primitive variables. The latter are calculated with a standard linear FE interpolation in each element:

$$\nabla\tilde{\mathbf{P}} = \frac{1}{2\Omega} \frac{\partial \tilde{\mathbf{P}}}{\partial \mathbf{P}} \sum_{j=1}^{3} \mathbf{P}_j\, \mathbf{n}_j, \tag{3.28}$$

where $\frac{\partial \tilde{\mathbf{P}}}{\partial \mathbf{P}}$ is the jacobian of the transformation from the update variables $\mathbf{P}$ (the ones in which the solution is stored, i.e. the ones for which a linear representation in the element

is assumed) to the primitive variables $\tilde{\mathbf{P}}$, whose gradients appear in the definition of the physical diffusive flux. For example, in the case of flows in thermo-chemical nonequilibrium, the physical diffusive fluxes require the gradients of mass fractions y_s, while the update variables provide the partial densities ρ_s, together with the velocity components and the temperatures:

$$\mathbf{P}=[\rho_s\ \mathbf{u}\ T\ T_v],\ \ \tilde{\mathbf{P}}=[y_s\ \mathbf{u}\ T\ T_v]. \tag{3.29}$$

As a result, given that $y_s=\rho_s/\rho$, the matrix $\frac{\partial\tilde{\mathbf{P}}}{\partial\mathbf{P}}$ reduces to:

$$\frac{\partial\tilde{\mathbf{P}}}{\partial\mathbf{P}}=\begin{pmatrix}(\delta_{ij}-y_i)/\rho & 0 & 0 & 0\\ 0 & 1 & 0 & 0\\ 0 & 0 & 1 & 0\\ 0 & 0 & 0 & 1\end{pmatrix}. \tag{3.30}$$

An alternative approach consists in computing the gradient of $\tilde{\mathbf{P}}$ directly from the nodal values of $\tilde{\mathbf{P}}$:

$$\nabla\tilde{\mathbf{P}}=\frac{1}{2\Omega}\sum_{j=1}^{3}\tilde{\mathbf{P}}(\mathbf{P}_j)\ \mathbf{n}_j. \tag{3.31}$$

The latter way of calculating the gradient is more straightforward and computationally efficient than the former, but, in our opinion, formally less consistent, because it does not use directly the variables $\mathbf{P}$, actually storing the solution. Moreover, since $\tilde{\mathbf{P}}(\mathbf{P})$ is nonlinear in $\mathbf{P}$, the two formulations in (3.28) and (3.31) cannot be considered equivalent.

Recently, different methods have been proposed for discretizing diffusive terms more consistently within a Residual Distribution framework. In [33], for example, a blended discretization based on the local Peclet number is designed in order to preserve uniform second order accuracy at low Peclet numbers, corresponding to diffusion-dominated flows. In [9], a value of Peclet number equal to 7 is suggested as threshold for determining when the use of the blending may be beneficial in compressible Navier-Stokes computations. As shown in Fig. 4, the local cell-based Peclet number is almost everywhere bigger than 7 in the numerical solution over the double cone, so that the use of an unmodified standard Galerkin approximation appears to be reasonably well motivated in this case. The latter assumption is confirmed by the high accuracy in the numerical prediction of the quantities of interest, in particular of the surface heat flux, as presented in the results section.

A more innovative and interesting idea has been introduced in [22,23] where the original equations for scalar advection-diffusion problems are recast into a first order system and a unified discretization is applied to the resulting fully hyperbolic system. An application to the Navier-Stokes equations has been already presented in [24] within a Finite Volume framework and shows promising results. However, an extension to more complex systems of equations, like the ones considered in this paper, if ever possible, might be far from trivial and not necessarily advantageous, due to an expected significant increase in number of equations to solve (i.e. one additional equation per diffusion coefficient).

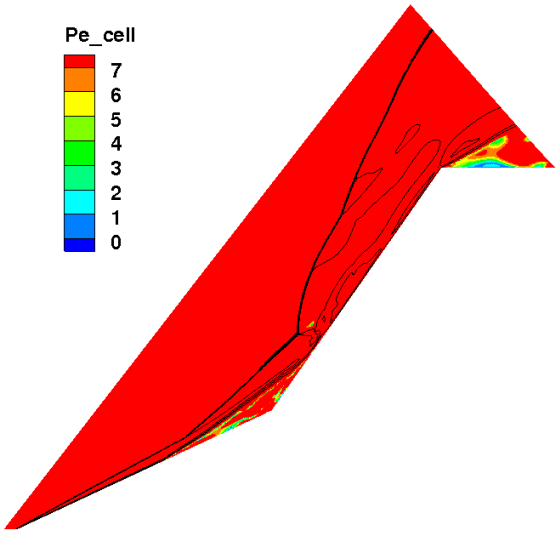

Figure 4: Cell Peclet number contours superposed on Mach isolines in the computed flowfield over the analyzed double cone configuration. The red region corresponds to a Peclet number ≥ 7.

Moreover, it is not clear yet how to integrate the discretization of nonlinear source terms into this approach consistently.

3.4 Source term discretization

If a variational formulation is applied to the source term $\mathbf{S}$ in (2.7) within the computational domain Ξ, its contribution to the nodal residual, as in the semi-discretized form in (3.2), can be expressed as [8]:

$$\mathbf{\Phi}_l^s = \sum_{\Omega \in \Xi_l} \int_\Omega \mathbf{w}_l^\Omega \, \mathbf{S} \, d\Omega. \tag{3.32}$$

A quadrature rule for discretizing the volume integral in (3.32) must be specified. The simplest possible choice is a one-point quadrature rule which leads to:

$$\mathbf{\Phi}_l^s = \sum_{\Omega \in \Xi_l} \mathbf{w}_l^\Omega(\mathbf{x}_c) \, \mathbf{S}(\mathbf{x}_c) \, \Omega = \sum_{\Omega \in \Xi_l} \mathbf{B}_l^\Omega \, \mathbf{S}_c \, \Omega, \tag{3.33}$$

where $\mathbf{x}_c$ is the centroid of the simplex element and $\mathbf{B}_l^\Omega = \frac{1}{\Omega} \int_\Omega \mathbf{w}_l^\Omega \, d\Omega$ is the distribution matrix. (3.33) shows that the source term can be distributed exactly like the convective term, at least if a distribution matrix can be defined for the convective scheme. Typically, the LDA distribution matrix is applied to distribute the source term [8]:

$$\mathbf{\Phi}_l^s = \sum_{\Omega \in \Xi_l} \mathbf{B}_l^{LDA,\Omega} \, \mathbf{S}_c \, \Omega. \tag{3.34}$$

In the case of the Nc and the Bxc schemes, the latter choice also corresponds to upwind the source term together with the convective fluctuation. To demonstrate this for the Nc scheme, the sum of the nodal convective and source term residuals distributed from one element is considered. After having recalled (3.13) and (3.15), the following relation holds:

$$\begin{aligned}(\boldsymbol{\Phi}_l^c-\boldsymbol{\Phi}_l^s)^\Omega &= \boldsymbol{\Phi}_l^{Nc}|_{\boldsymbol{\Phi}^{c,\Omega}}-\mathbf{B}_l^{LDA}\mathbf{S}_c\\ &= \boldsymbol{\Phi}_l^N+\mathbf{B}_l^{LDA}\,\delta\boldsymbol{\Phi}^{c,\Omega}-B_l^{LDA}\mathbf{S}_c\\ &= \boldsymbol{\Phi}_l^N+\mathbf{B}_l^{LDA}(\boldsymbol{\Phi}^{c,\Omega}-\tilde{\boldsymbol{\Phi}}^{c,\Omega})-\mathbf{B}_l^{LDA}\mathbf{S}_c\\ &= \boldsymbol{\Phi}_l^N+\mathbf{B}_l^{LDA}(\boldsymbol{\Phi}^{c,\Omega}-\mathbf{S}_c-\tilde{\boldsymbol{\Phi}}^{c,\Omega})\\ &= \boldsymbol{\Phi}_l^{Nc}|_{\boldsymbol{\Phi}^{c,\Omega}-\mathbf{S}_c}.\end{aligned} \tag{3.35}$$

This result is indeed identical to (3.20). The same analogy holds for the Bxc scheme:

$$\begin{aligned}(\boldsymbol{\Phi}_l^c-\boldsymbol{\Phi}_l^s)^\Omega &= \boldsymbol{\Phi}_l^{Bxc}|_{\boldsymbol{\Phi}^{c,\Omega}}-\mathbf{B}_l^{LDA}\mathbf{S}_c\\ &= (1-\Theta)\,\boldsymbol{\Phi}_l^{LDAc}+\Theta\boldsymbol{\Phi}_l^{Nc}-\mathbf{B}_l^{LDA}\mathbf{S}_c\\ &= (1-\Theta)\,\mathbf{B}_l^{LDA}\boldsymbol{\Phi}^{c,\Omega}+\Theta\boldsymbol{\Phi}_l^{Nc}-\mathbf{B}_l^{LDA}\mathbf{S}_c\\ &= (1-\Theta)\,\mathbf{B}_l^{LDA}(\boldsymbol{\Phi}^{c,\Omega}-\mathbf{S}_c)+\Theta(\boldsymbol{\Phi}_l^{Nc}-\mathbf{B}_l^{LDA}\mathbf{S}_c)\\ &= (1-\Theta)\,\boldsymbol{\Phi}_l^{LDAc}|_{\boldsymbol{\Phi}^{c,\Omega}-\mathbf{S}_c}+\Theta\boldsymbol{\Phi}_l^{Nc}|_{\boldsymbol{\Phi}^{c,\Omega}-\mathbf{S}_c}\\ &= \boldsymbol{\Phi}_l^{Bxc}|_{\boldsymbol{\Phi}^{c,\Omega}-\mathbf{S}_c}.\end{aligned} \tag{3.36}$$

3.5 Backward Euler time integration

After having applied the CRD discretization to the spatial term of (3.2), the system can be rewritten as

$$\frac{\partial\mathbf{U}}{\partial\mathbf{P}}\frac{\partial\mathbf{P}}{\partial t}+\mathbf{R}^{\mathcal{CRD}}(\mathbf{U})=0=\tilde{\mathbf{R}}(\mathbf{P}), \tag{3.37}$$

where $\tilde{\mathbf{R}}(\mathbf{P})$ is a *pseudo-steady* residual and $\mathbf{P}$ is the previously introduced vector of natural variables, which represents a convenient way for storing the solution. The choice of a Backward Euler time integrator leads to the following expression for the residual $\tilde{\mathbf{R}}(\mathbf{P})$:

$$\tilde{\mathbf{R}}(\mathbf{P})=\frac{\mathbf{U}(\mathbf{P})-\mathbf{U}(\mathbf{P}^n)}{\Delta t}\Omega+\mathbf{R}^{\mathcal{CRD}}(\mathbf{P}), \tag{3.38}$$

where Ω is the area of the median dual cell and $\mathbf{U}=\mathbf{U}(\mathbf{P})$ is an explicit analytical relation, i.e. the transformation from natural to conservative variables. The application of a one step Newton method yields the following linear system:

$$\left[\frac{\partial\tilde{\mathbf{R}}}{\partial\mathbf{P}}(\mathbf{P}^n)\right]\Delta\mathbf{P}^n=-\tilde{\mathbf{R}}(\mathbf{P}^n), \tag{3.39}$$

where the jacobian matrix $\frac{\partial\tilde{\mathbf{R}}}{\partial P}$ is computed as:

$$\frac{\partial\tilde{\mathbf{R}}}{\partial\mathbf{P}}=\frac{\partial\mathbf{U}}{\partial\mathbf{P}}(\mathbf{P})\frac{\Omega}{\Delta t}+\frac{\partial\mathbf{R}^{\mathcal{CRD}}}{\partial\mathbf{P}}. \tag{3.40}$$

Herein, the jacobian matrix of the spatial part of the residual, $\frac{\partial\mathbf{R}^{\mathcal{CRD}}}{\partial\mathbf{P}}$, is evaluated numerically by perturbing the space residual $\mathbf{R}$ with respect to each one of the natural variables. The solution update is also performed in natural variables.

3.5.1 Strong implicit boundary conditions

All boundary conditions, namely supersonic inlet, symmetry and no-slip isothermal wall are enforced strongly, so that each nodal state b on the boundary obeys the prescribed conditions. In particular, in the case of the no-slip wall with imposed temperature, the condition to impose is

$$\mathbf{u}_b=0,\qquad T_b=T_b^v=T_w. \tag{3.41}$$

Since the natural variables $\mathbf{P}$ are used for both the solution update and the numerical perturbation of the residual, the implicit treatment of such a boundary condition translates into replacing the rows corresponding to the variables $\mathbf{u},T,T^v$ for the wall nodes b of the jacobian matrix $\frac{\partial\tilde{\mathbf{R}}}{\partial\mathbf{P}}$ with

$$K_b\,\Delta\mathbf{u}_b=0,\qquad K_b\,\Delta T_b=0,\qquad K_b\,\Delta T_b^v=0, \tag{3.42}$$

where K_b is the coefficient used to enforce the CFL condition for the corresponding explicit scheme [6], including both an advective and a diffusive contributions, and is calculated as

$$K_b=\frac{\Omega_b}{\Delta t}=\frac{1}{CFL}\left(\sum_{\Omega\in\Xi_b}\frac{1}{2}(\bar{\lambda}^+_{\max})_b^\Omega\|\mathbf{n}_b^\Omega\|+\sum_{\Omega\in\Xi_b}\frac{\bar{\nu}\|\mathbf{n}_b^\Omega\|^2}{2^2\,\Omega}\right). \tag{3.43}$$

In (3.43), $(\bar{\lambda}^+_{\max})_b^\Omega$ is the linearized maximum positive eigenvalue, $\bar{\nu}$ is the cell averaged kinematic viscosity, $\mathbf{n}_b^\Omega$ is the inward normal corresponding to node b inside cell Ω. K_b is used for scaling purposes here, in order to keep a good conditioning number of the system matrix when approaching convergence, since $\lim_{\Delta t\to\infty}K_b=0$.

If a non-catalytic condition is used, as in the present case, the jacobian rows corresponding to the partial densities of the wall nodes do not need any modification.

4 Numerical results

The Residual Distribution based model presented so far has been targeted towards the the simulation of axisymmetric double cone flows in thermo-chemical nonequilibrium conditions. In order to validate the method, the high-enthalpy (9.17 MJ/kg) and high-speed ($M_\infty=11.5$) nitrogen flow over a double cone with semi angles of 25^o and 55^o and a base diameter of 10.3 inches, as shown in Fig. 5 (left), was chosen.

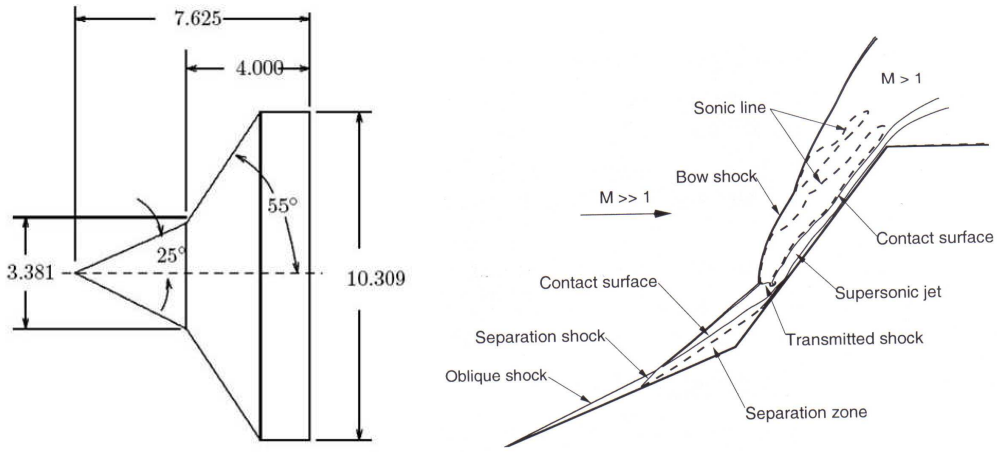

Figure 5: Double cone geometry with lengths given in inches (left) and schematic of double-cone flowfield in run 42 (right) at high free stream enthalpy conditions (courtesy from [26]).

This configuration has been analyzed within the RTO Task Group 43 (topic no 2) [15], which focused on a further assessment of CFD for the specific issue of shock interactions and control surfaces in nonequilibrium flows. Extensive experimental studies have also been conducted for this case in the LENS I shock tunnel at Calspan University of Buffalo Research Center (CUBRC) to obtain detailed surface and flow characteristics.

A sketch of a typical hypersonic flowfield around a double cone is depicted in Fig. 5 (right). The oblique shock generated by the first cone strongly interacts with the detached bow shock created on the second one and the resulting transmitted shock impinges on the surface downstream of the cone-cone juncture. Here, the adverse pressure gradient forces the boundary layer to separate. This causes the appearance of a separation shock, which interacts with the bow shock and causes a shift of the interaction point, which in turns alters the separation zone. This process feeds back on itself until the flow reaches a steady state, if such a state exists. Moreover, a supersonic jet forms along the surface of the second cone, downstream of the impingement point, and it undergoes a series of compressions and expansions [26].

An accurate prediction of the aerodynamic field and related quantities (heat flux) for hypersonic double cone flows requires thermo-chemical nonequilibrium effects to be taken into account, as demonstrated in [18,25,26]. All those effects have indeed been accounted for in the present work, thanks to the state-of-the-art two-temperature nonequilibrium model described in Section 2. Both reference literature and experimental data were available for the selected testcase, indicated as *run 42* in [26]. The nominal free stream conditions are listed in Table 1. Additionally, the wall temperature was set to 294.7 K.

The two-species ($N-N_2$) nitrogen mixture described in [26] was used to model the chemistry. Only the second order accurate results, computed with the Bxc scheme defined in (3.21), are discussed here. Since the CRD method is based on simplex cells (tri-

Table 1: Free stream conditions for double cone (run 42).

$\rho_\infty[kg/m^3]$	$U_\infty[m/s]$	$T_\infty[K]$	$T_\infty^v[K]$	y_N	y_{N_2}
0.001468	3849.3	268.7	3160	0	1

angles in 2D or tetrahedra in 3D), the original intermediate structured mesh used in [26] (256×512 cells) has been split into triangles. With regard to this, some details of a coarser computational mesh (half grid points in both directions) are presented in Fig. 6, showing the regions around the tip of the first cone and around the junction between the two cones respectively.

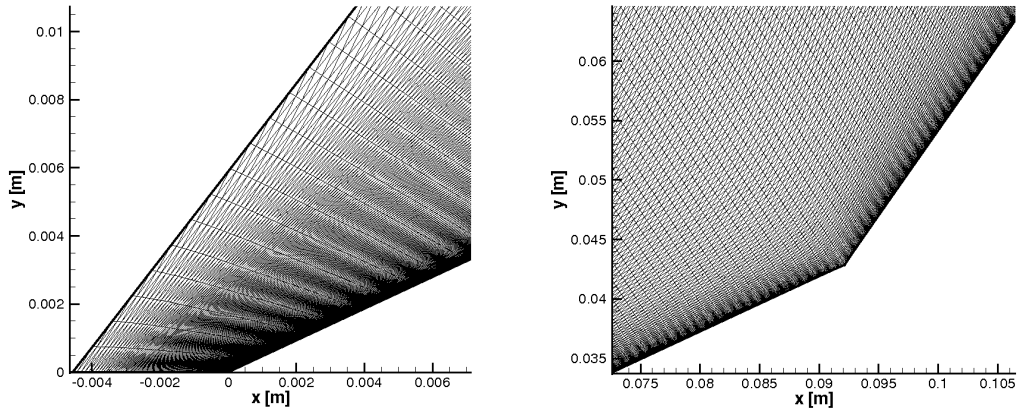

Figure 6: Mesh views around the tip of the first cone (left) and around the junction between the two cones (right).

From the Mach number and roto-translational temperature contours/isolines in Fig. 7 the excellent shock capturing properties of the CRD method can be seen. The vibrational temperature of molecular nitrogen is shown in Fig. 8, clearly indicating a non-negligible presence of thermal nonequilibrium in the flow, particularly in the boundary layer and downstream the bow shock, where the roto-translational temperature is higher. Only a moderate dissociation of molecular nitrogen into atoms occurs, as highlighted from the contours/isolines of atomic nitrogen mass fractions. Because of the effect of the vibration-dissociation coupling, the regions characterized by the highest vibrational temperature exhibit more chemical dissociation.

Figs. 9 and 10 (left) show the comparison between experimental and computed heat flux and surface pressure. Specifically the latter quantities, which are of actual engineering interest, demonstrate the accurate prediction capabilities of the CRD solver. Those results are competitive with the grid-converged results provided by [26] (right pictures in Figs. 9 and 10) obtained with a state-of-the-art second order FV solver on a much finer mesh (512×1024 quadrilateral cells), containing approximately four times more degrees of freedom than in our case.

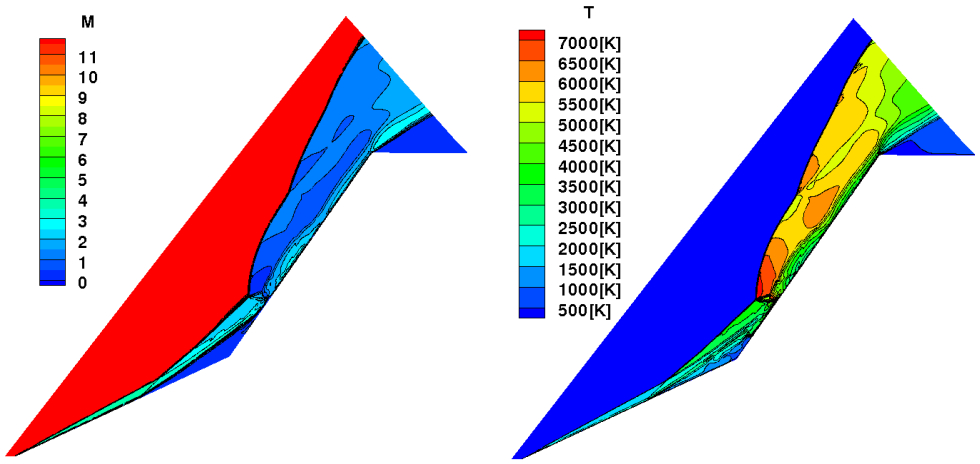

Figure 7: Contours/isolines of Mach number (left) and roto-translational temperature (right) computed with Bxc scheme on the double cone.

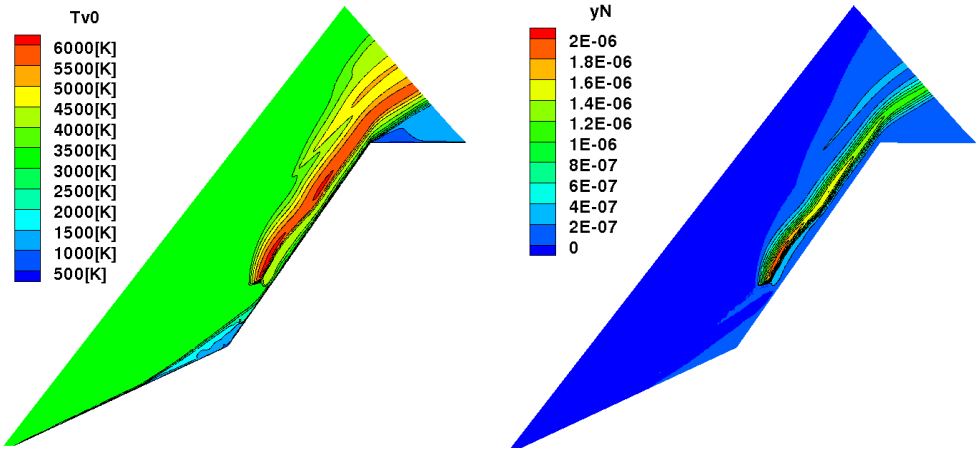

Figure 8: Contours/isolines of vibrational temperature of N_2 (left) and mass fraction of atomic nitrogen N (right) computed with Bxc scheme on the double cone.

A partial grid convergence has been performed by comparing the previously discussed results with those obtained on a coarser mesh (half grid points in both directions). In both cases, first and second order solutions are considered and they are shown in Fig. 11 in terms of surface pressure and heat flux distribution. The solution computed with the Bxc scheme is significantly closer to the experimental data than the results given by the Nc scheme, on both meshes, except for the peak pressure on the coarse mesh, which is excessively high in the second order solution. Both schemes provide a considerably more accurate solution on the fine mesh which demonstrates a correct trend towards grid convergence. This is particularly evident in the size of the separation bubble, the peak pressure and the peak heat flux.

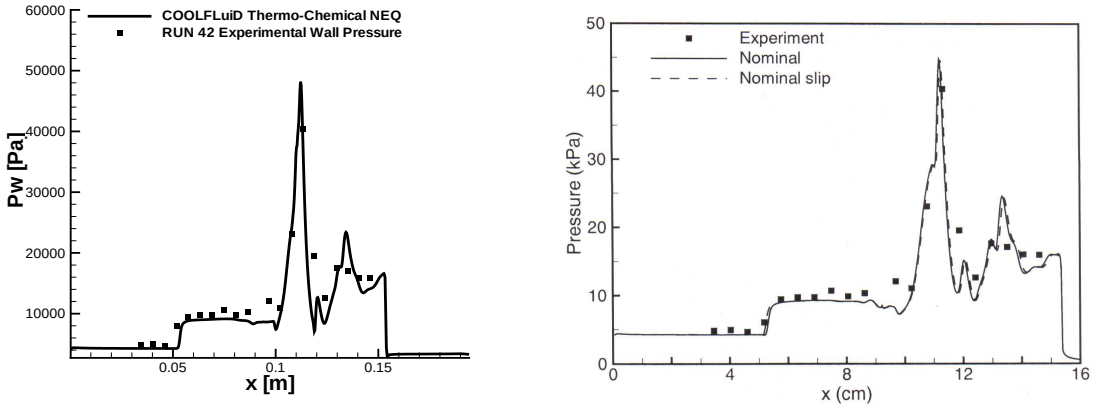

Figure 9: Computed surface pressure vs. experimental measurements, Bxc (left) on 256×512 DOF mesh of triangles vs. [26] (right) on 512×1024 DOF mesh of quadrilaterals.

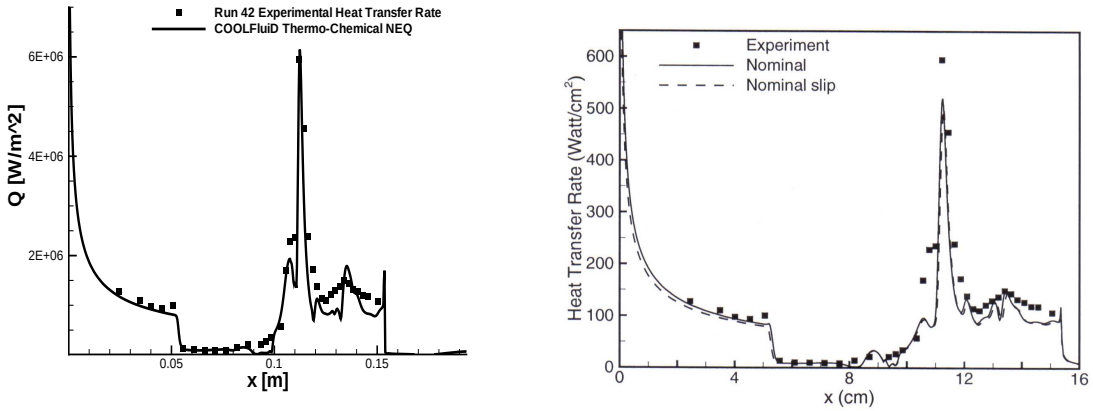

Figure 10: Computed surface heat flux vs. experimental measurements, Bxc (left) on 256×512 DOF mesh of triangles vs. [26] (right) on 512×1024 DOF mesh of quadrilaterals.

Fig. 12 shows the convergence history for the computation with the first order Nc scheme on the fine mesh in terms of roto-translational and vibrational temperatures, surface pressure and heat flux: this computation took approximately 10 hours running on 64 CPUs and converged nicely in about 8,000 iterations. As shown in the same picture, the CFL was progressively increased from 0.5 to 200.

The resulting solution was fed as initial field to the second order simulation. In the latter case, the residuals quickly stalled after a drop of 1-2 orders of magnitude (depending on the variable). The total run took about a month on 128 CPUs and was stopped after more than 2,000,000 iterations, once the surface pressure distribution (and in particular the separation bubble size) and the surface heat flux stopped changing. The maximum

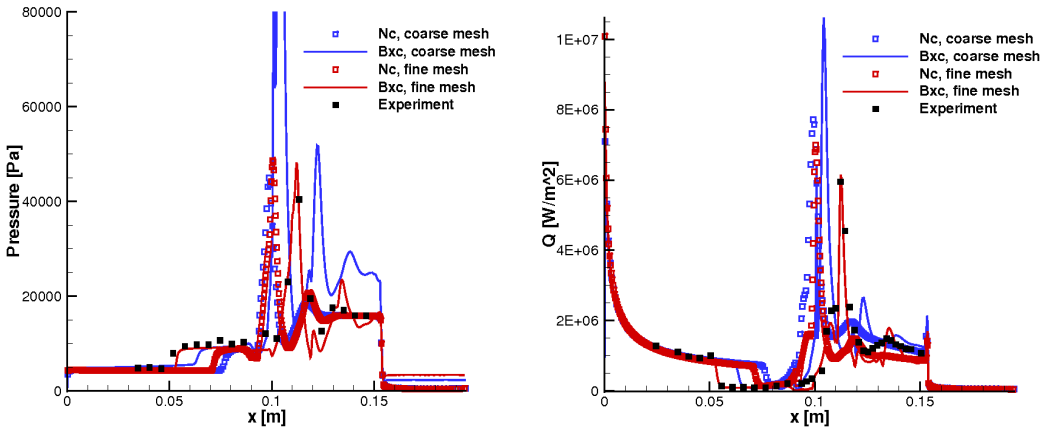

Figure 11: Grid convergence study showing surface pressure (left) and heat flux (right) on coarse (128×256 DOFs) and fine (256×512 DOFs) meshes. Solutions with first order Nc scheme, second order Bxc and experiments are compared.

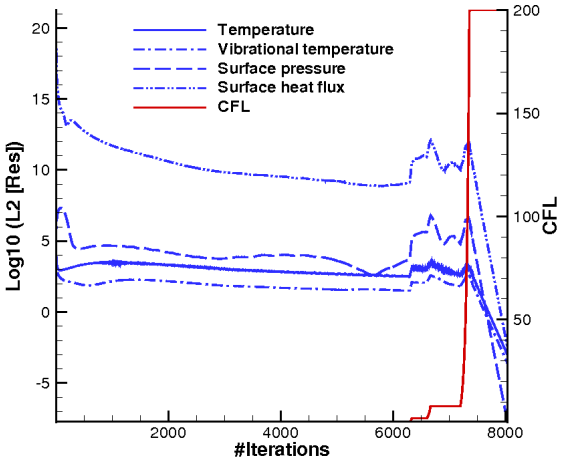

Figure 12: Convergence histories in terms of CFL law, temperatures, surface pressure and heat flux residuals versus number of iterations.

allowable CFL was limited to 15. Such a long running time is not due to the method itself, but to some computationally expensive (but supposedly more accurate) models used for computing transport (e.g. Stefan-Maxwell's diffusion fluxes) and thermodynamic properties.

In the second order simulation (both on the coarse and fine meshes), probably due to the non-strictly positive nature of the scheme, overshoots in temperature appeared in a few grid points located near the bow shock on the second cone. Therefore, the minimum allowable temperature had to be fixed to a positive value to prevent the simulation to blow up. This behaviour clearly contributed to severely hamper the convergence, whose improvement remains an open issue to be tackled by future research. This is mandatory

in order to make the CRD method fully competitive with standard numerical discretizations for those kind of applications.

5 Conclusion

A multidimensional upwind CRD method for simulating steady 2D axisymmetric viscous flows in thermo-chemical nonequilibrium on unstructured meshes has been presented in this paper. A second-order accurate scheme, based on the conservative, quasi-monotone, nonlinear Bxc scheme for distributing advective and source terms and a standard Galerkin approximation for discretizing the diffusive terms, has been applied to analyze a high-enthalpy double cone configuration for which both experimental measurements and scientific literature was available.

The promising numerical results here presented show the high accuracy of the RD algorithm, even on relatively coarse meshes, and, therefore, its high potential for better resolving hypersonic chemically reacting flows characterized by complex shock wave boundary layer interactions (SWBLI). This confirms RD as a possible valid alternative to FV for those kind of applications. Future work will be focused on improving the convergence of the Bxc scheme, which has showed some deficiencies.

References

[1] Barbante, P. F., Degrez, G., and Sarma, G. S. R., Computation of Nonequilibrium High-Temperature Axisymmetric Boundary-Layer Flows, J. Thermophys. Heat Transfer, Vol. 16 (2002), No. 4, pp. 490–497.

[2] Bottin, B., Vanden Abeele, D., Carbonaro, M., Degrez, G., and Sarma, G. S. R., Thermodynamic and Transport Properties for Inductive Plasma Modeling, J. Thermophys. Heat Transfer, Vol. 13 (1999), pp. 343–350.

[3] Candler, G. V. and MacCormack, Computation of Weakly Ionized Hypersonic Flows in Thermochemical Nonequilibrium, J. Thermophys. Heat Transfer, Vol. 5, No. 11 (1991), pp. 266–273.

[4] Ćsik, *Á*., Upwind Residual Distribution Schemes for General Hyperbolic Conservation Laws and Application to Ideal Magnetohydrodynamics,Ph.D. thesis, Katholieke Universiteit Leuven, Faculteit Wetenschappen Centrum voor Plasma-Astrofysica, Belgium, 2002.

[5] Ćsik, *Á*., Ricchiuto, M., Deconinck, H., A conservative formulation of the multidimensional upwind residual distribution schemes for general nonlinear conservation laws, J. Comput. Phys., Vol. 179, No. 2 (2002), pp. 286–312.

[6] Deconinck, H., Ricchiuto, M., Sermeus, K., Introduction to residual distribution schemes and stabilized finite elements, VKI LS 2003-05, 33^{rd} Computational Fluid Dynamics Course, von Karman Institute for Fluid Dynamics, 2003.

[7] Deconinck, H., Roe, P. L., Struijs, R., A multidimensional generalization of Roe's difference splitter for the Euler equations, Computer and Fluids, Vol. 22, No. 2/3 (1993), pp. 215–222.

[8] Degrez, G., van der Weide E., Upwind residual distribution schemes for chemical non-equilibrium flows, Paper 99-3366, 14th AIAA Computational Fluid Dynamics Conference, Norfolk, USA, June 28–July 1, 1999.

[9] Dobeš J., Numerical Algorithms for the Computation of Unsteady Compressible Flows over Moving Geometries. Applications to Fluid-Structure Interaction, PhD thesis submitted at Czech Technical University, Prague, Czech Republic, Université Libre de Bruxelles, Belgium, November 2007.
[10] Dobeš J. and Deconinck H., A Shock Sensor-Based Second-Order Blended (Bx) Upwind Residual Distribution Scheme for Steady and Unsteady Compressible Flow, in Hyperbolic Problems: Theory, Numerics, Applications, 978-3-540-75711-5 (print), 978-3-540-75712-2 (online), pp. 465-473, 2008, Springer Berlin Heidelberg.
[11] Gnoffo, P. A., Gupta, R. N., and Shinn, J. L., Conservation equations and physical models for hypersonic air flows in thermal and chemical non-equilibrium. Technical Paper 2867, NASA, 1989.
[12] Gupta, R. N., Yos, J. M., Thompson, R. A., and Lee, K. P., A review of reaction rates and thermodynamic and transport properties for an 11-species air model for chemical and thermal non-equilibrium calculations to 30 000 K. Reference Publication 1232, NASA, August 1990.
[13] Hirschfelder, J. O., Curtiss, C. F. and Bird, R. B., Molecular theory of gases and liquids, Wiley, New York, 1954.
[14] Issmann, E., Degrez, G., Deconinck, H., Implicit upwind residual distribution Euler and Navier-Stokes solver on unstructured meshes, AIAA Journal, Vol. 34 (1996), pp. 2021–2028.
[15] Knight, D., Longo, J., Drikakis, D., Gaitonde, D., Lani, A., Nompelis, I., Reimann, B. and Walpot, L., Assessment of CFD Capability for Prediction of Hypersonic Shock Interactions, Prog. Aerospace Sci., to appear.
[16] Lani, A., Quintino, T., Kimpe, D., Deconinck, H., Vandewalle, S., Poedts, S., The COOLFluiD Framework: Design Solutions for High-Performance Object Oriented Scientific Computing Software, Computational Science - ICCS 2005, LNCS 3514, Springer-Verlag, Vol. 1 (2005), pp. 281–286.
[17] Lani, A., Quintino, T., Kimpe, D., Deconinck, H., Vandewalle, S., Poedts, S., Reusable Object-Oriented Solutions for Numerical Simulation of PDEs in a High Performance Environment, Scientific Programming, ISSN 1058-9244, IOS Press, Vol. 14, No. 2 (2006), pp. 111-139.
[18] MacLean, M., Holden, M., Wadhams, T. and Parker R., A computational analysis of thermochemical studies in the lens facilities. ph45th AIAA Aerospace Sciences Meeting and Exhibit, Reno, Nevada (US), AIAA 207-121, Jan 2007.
[19] Magin, T. E., Degrez, G., Transport algorithms for partially ionized unmagnetized plasmas, J. Comput. Phys., Vol. 198 (2004), pp. 424–449.
[20] Magin, T. E., Degrez, G., Transport properties for partially ionized unmagnetized plasmas, Phys. Rev. E, Vol. 70 (2004).
[21] Millikan, R. C. and White, D. R., Systematics of vibrational relaxation. J. of Chem. Phys., Vol. 39, No. 12 (1963), pp. 3209–3213.
[22] Nishikawa, H., A First-Order System Approach for Diffusion Equation. I: Second-Order Residual Distribution Schemes, J. Comput. Phys., 227 (2007), pp. 315-352.
[23] Nishikawa, H., A First-Order System Approach for Diffusion Equation. II: Unification of Advection and Diffusion, J. Comput. Phys., 229 (2010), pp. 3989-4016.
[24] Nishikawa, H., New-Generation Hyperbolic Navier-Stokes Schemes: (1/h) Speed-Up and Accurate Viscous/Heat Fluxes, AIAA Paper 2011-3043, 20th Computational Fluid Dynamics Conference, June 2011.
[25] Nompelis, I., Drayna T. W and Candler G. V., A Parallel Implicit Solver for Hypersonic Reacting Flow Simulation, AIAA 2005-4867, 17th AIAA Computational Fluid Dynamics Conference, Toronto, Canada, June 6-9, 2005.

[26] Nompelis, I., Computational Study of Hypersonic Double-Cone Experiments for Code Validation, PhD Thesis, University of Minnesota, May 2004.
[27] Paillere, H., phMulti-dimensional Upwind Residual Distribution Schemes for the Euler and Navier-Stokes Equations on Unstructured Grids. PhD thesis, Universit*é* Libre de Bruxelles, 1995.
[28] Park, C., Nonequilibrium Hypersonic Aerothermodynamics, John Wiley and Sons, New York, 1989.
[29] Park, C., Review of Chemical-Kinetic Problems of Future NASA Mission, I: Earth Entries, J. Thermophys. Heat Transfer, Vol. 7 (1993), pp. 385–398.
[30] Argonne National Laboratory: PETSc. Portable, Extensible Toolkit for Scientific Computation, `http://www-unix.mcs.anl.gov/petsc`, 2004.
[31] Prabhu, R. K., An implementation of a Chemical and Thermal Nonequilibrium Flow Solver on Unstructured Meshes and Application to Blunt Bodies, NASA Contractor Report 194967, Lockheed Engineering and Sciences Co., Hampton, VA, August 1994.
[32] Ricchiuto, M., Construction and Analysis of Compact Resdidual Discretizations for Conservation Laws on Unstructured Meshes, Ph.D. thesis, Universit*é* Libre de Bruxelles, 2005.
[33] Ricchiuto, M., Villedieu, N., Abgrall, R., and Deconinck, H., On uniformly high order accurate residual distribution schemes for advection-diffusion, J. Comput. Applied Math., Vol. 215 (2007), pp. 547–556.
[34] Sarma, G. S. R., Physico-chemical modeling in hypersonic flow simulation, Prog. Aerospace Sci., pp. 281–349, 1958.
[35] Sutton, K. and Gnoffo, P. A., Multi-component diffusion with application to computational aerothermodynamics, Technical Paper 98-2575, AIAA, Albuquerque, New Mexico, June 1998.
[36] Van der Weide, E., Deconinck, H., Issmann, E., Degrez, G., A parallel implicit multidimensional upwind residual distribution method forthe Navier-Stokes equations on unstructured grids, J. Comp. Mech., Vol. 23 (1999), No. 2, pp. 199–208.
[37] Van der Weide, E., Compressible Flow Simulation on Unstructured Grids using Multidimensional Upwind Schemes, Ph.D. thesis, Delft University of Technology, Netherlands, 1998.
[38] Yos, J. M., Approximate equations for the viscosity and translational thermal conductivity of gas mixtures, Contract Report AVSSD-0112-67-RM, AVCO Corp., Wilmington, MA, 1967.